Microelectronics Journal 151 (2024) 106300

Contents lists available at ScienceDirect

Microelectronics Journal

journal homepage: www.elsevier.com/locate/mejo

A novel design method for wideband bandpass filters with fewer inductors☆

Jialong Xin, Yazi Cao *, Hangxing Li, Mingzhao Xu, Gaofeng Wang **

MOE Engineering Research Center of Smart Microsensors and Microsystems, the School of Electronics and Information, Hangzhou Dianzi University, Hangzhou City, Zhejiang Province, 310018, China

ARTICLE INFO

Index Terms:
Band-pass filter (BPF)
Improvement
Non-resonator
Transformed
Transmission zero

ABSTRACT

Inductors that are widely used in wideband filter designs could result in large filter size and high insertion loss. A novel design method using admittance matrix based on direct circuit implementation is introduced for wideband bandpass filters. Firstly, a frequency transformation is performed on cross-couplings to realize the conversion between inductor and capacitor, thereby reducing usage of inductors. Moreover, by virtue of an enhanced resonator (type I), an approach of adding extra transmission zero is proposed to improve the out-of-band rejection without any additional usage of inductors. Thirdly, based on the frequency transformation, another enhanced resonator (type II) is introduced to further improve the frequency characteristics without compromising usage of inductors. Finally, by cascading the enhanced resonators of type I and type II, a novel filter can be constructed. This novel filter is designed and fabricated using a glass-based integrated passive device (IPD) technology. The measurement results are highly consistent with the simulation results. It is shown that the proposed design method can reduce the filter size and thus improve the chip integration. It enriches the freedoms during the filter design.

1. Introduction

RF front-end module is an important part of a wireless communication systems, which is responsible for processing RF signals [1,2]. Rejecting unwanted and spurious signals is usually accomplished by miniaturized microwave bandpass filters, which is part of the RF front-end module. Modern wireless communication systems have put forward higher requirements for filter performance, especially insertion loss, out-of-band suppression, and size. Acoustic filters including surface acoustic filters (SAW) and bulk acoustic wave (BAW) filters have been used in RF front-ends, with small size, high out-of-band rejection, and low insertion loss [3,4]. Limited by the energy conversion efficiency of resonators, it is difficult for acoustic filters to achieve a wide passband and be applied to higher frequencies.

Filters based on low-temperature cofired ceramic (LTCC) [5] technology and integrated passive device (IPD) [6] technology are also used in RF front-ends. Compared with acoustic filters, IPD filters can achieve a wider bandwidth and perform better at high frequencies. The IPD process based on the glass or silicon is more precise than LTCC and has a thinner thickness, which makes it easier to be integrated [7–9]. However, IPD technology has higher insertion loss. How to reduce the insertion loss of IPD filters is a key issue to be resolved.

Matrix synthesis is an important tool for filter design. Chebyshev polynomials provided a synthesis method for filter design [10]. In recent years, many novel filter synthesis methods have been proposed, such as multiband coupling matrix synthesis technique [11,12], lossy microwave filter coupling matrix synthesis method [13,14], coupling matrix with non-resonator [15,16], three-dimensional coupling matrix technology [17], coupling matrix with nonreciprocal filter [18,19], and coupling matrix with frequency-dependent coupling [20,21]. Due to the use of constant coupling coefficients, these coupling coefficients need to be determined at the center frequency, which makes the synthesized filters narrow-band.

In order to achieve wideband filters, a method to determine the resonators and inverters with acceptable quality factors by adjusting the normalized slope parameter or the reference susceptance parameter has been proposed [22]. Moreover, based on the theory in Ref. [23], a method for converting negative lumped element into positive lumped

☆ This work was supported by National Natural Science Foundation of China under Grants 92373202 and 62141409, National Key Research and Development Program of China under Grant 2019YFB2205003, and Zhejiang Provincial Key Research & Development Project under Grant 2021C01041.

* Corresponding author.
** Corresponding author.
E-mail addresses: caoyazi@hdu.edu.cn (Y. Cao), gaofeng@hdu.edu.cn (G. Wang).

https://doi.org/10.1016/j.mejo.2024.106300
Received 9 May 2024; Received in revised form 19 June 2024; Accepted 2 July 2024
Available online 17 July 2024

element was presented in Ref. [24]. Although these methods can produce wideband filters, a large number of inductors were used, and thus resulting in large filter size and high insertion loss.

In this work, a new filter design method is proposed to resolve the issue of excessive inductor usage. This method is an improvement of the cascade filter design directly implemented by lumped elements. A frequency transformation and two enhanced resonators are proposed in this design method. The wideband bandpass filters (BPFs) with a small number of inductors are realized from the coupling matrix by virtue of this design method, which offers a general approach for designing wideband BPFs with fewer inductors. To validate this design method, a novel filter is designed and fabricated using a glass-based IPD technology. The measurement results are highly consistent with the simulation results. It is shown that this design method can reduce the filter size and thus improve the chip integration. It enriches the freedoms during the filter design.

2. Proposed method

2.1. Coupling matrix

The admittance characteristics of a filter with n cascade resonators, as shown in Fig. 1(a), can be well characterized by an $(n+2)$ by $(n+2)$ matrix, called the coupling matrix A, as follows [23]:

$$A=\begin{bmatrix} -j & m_{S1} & \cdots & m_{Sn} & m_{SL} \\ m_{S1} & m_{11} & \cdots & m_{1n} & m_{1l} \\ \vdots & \vdots & \ddots & \vdots & \vdots \\ m_{Sn} & m_{1n} & \cdots & m_{nn} & m_{nL} \\ m_{SL} & m_{1l} & \cdots & m_{nL} & -j \end{bmatrix} \tag{1}$$

where m_{ii} is the self-coupling of the i th resonator, m_{ik} is the coupling between the i th and k th resonators. For a given filter topology, the matrix A can be obtained using synthesis method described in Ref. [23]. The S-parameters can be calculated in terms of matrix A as

$$\begin{aligned} S_{11} &= 1+2j\left[A^{-1}\right]_{11} \\ S_{12} &= S_{21} = -2j\left[A^{-1}\right]_{1,N+2} \end{aligned} \tag{2}$$

For a resonator consisting of a grounded parallel inductor and a capacitor as shown in Fig. 1(b), m_{ii} can be expressed as

$$m_{ii}=\omega C_i-\frac{1}{\omega L_i} \tag{3}$$

Considering the case where the circuit consists exclusively of lumped elements, J admittance inverter, as shown in Fig. 1(c)–is employed to describe the coupling between resonators, where Y in Fig. 1(c) is considered as an inductor, capacitor or resonator [25]. The coupling term m_{ik} can be expressed as the admittance of the lumped element Y in Fig. 1(c). Notice that there are two negative elements in the conductive inverter consisting of lumped elements in Fig. 1(c), which is absorbed by the resonator adjacent to the inverter. It's means that the resonance frequency of the resonator will change. Therefore, the resonator consisting of parallel inductors and capacitors need be compensated as

$$\begin{aligned} L_i &\leftarrow 1\Big/\left(\frac{1}{L_k}+\sum_{k=1}^{n}\frac{1}{L_{ik}}\right) \\ C_i &\leftarrow C_i+\sum_{k=1}^{n}C_{ik} \end{aligned} \tag{4}$$

where $i \neq k$. Noted that when there is only inductance coupling or capacitance coupling between resonator i and resonator k, the missing compensation should be omitted.

Without loss of generality, it is assumed that the source and load impedances are normalized, and the source and load are directly connected to one resonator only in all the derivations hereinafter.

2.2. Transformation

For cascade filters with most couplings being inductive, a lowpass to highpass transformation is introduced. This can be viewed as a quadratic transformation based on the lowpass prototype to the bandpass transformation. Give a mapping

$$-\frac{t}{\omega}\leftarrow\omega \tag{5}$$

where t is a real variable. This transformation is applied to the entire circuit, i.e., not only to the J-admittance inverter, but also to the resonator itself. For a resonator consisting of an inductor and a capacitor connected in parallel, this transformation does not change its resonance characteristics. Note that this transformation maps $\omega = 0$ to $\omega = \infty$, and $\omega = \infty$ to $\omega = 0$, the frequencies of the transmission zeros in the stopband and the poles of the passband are changed. Therefore, this transformation changes the passband of the filter.

The transformed transmission zeros and poles can be represented by variable t and the original frequency

$$\omega' = \frac{1}{t\omega} \tag{6}$$

The CT filter consisting of three resonators has three poles and a transmission zero, where the transmission zero is generated by cross-coupling. Consider the CT filter with two inductive coupling and one capacitive coupling in Fig. 2(a) as an illustration. Resonators 1 and 3 are directly connected to the source and load, respectively. To facilitate calculations, the impedances of the filter's source and load are normalized. Therefore, the constant external couplings m_{S1} and m_{3L} are equal to 1 and -1, respectively [21]. From (1), the coupling matrix of the third-order BPF in Fig. 2(a) can be expressed as

$$A=\begin{bmatrix} -j & 1 & 0 & 0 & 0 \\ 1 & m_{11} & m_{12} & m_{13} & 0 \\ 0 & m_{12} & m_{22} & m_{23} & 0 \\ 0 & m_{13} & m_{23} & m_{33} & -1 \\ 0 & 0 & 0 & -1 & -j \end{bmatrix} \tag{7}$$

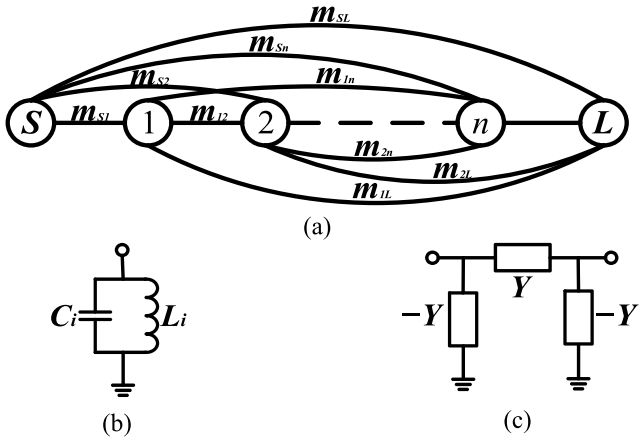

Fig. 1. (a) Filter with n resonators cascaded. (b) Resonator. (c) J admittance inverter.

Fig. 2. (a) CT filter with two inductive coupling and one capacitive coupling. (b) CT filter with one inductive filter and two capacitive coupling.

where

$$m_{12}=\frac{1}{\omega L_{12}}, m_{13}=\frac{1}{\omega L_{13}}, m_{23}=-\omega C_{23}$$

Following the mapping in (5), the inductive coupling m_{12}, and m_{13} can be transformed into capacitive as shown in Fig. 2(b). For the transformed filter, the elements in its coupling matrix should be modified as

$$m_{ii}{}'=\frac{\omega}{tL_i}-\frac{tC_i}{\omega}, m_{12}{}'=-\frac{\omega}{tL_{12}}$$

$$m_{13}{}'=-\frac{\omega}{tL_{13}}, m_{23}{}'=\frac{tC_{23}}{\omega} \tag{8}$$

Comparing with the filter in Fig. 2(a), the filter in Fig. 2(b) uses one less inductor. For circuits with far more inductors than capacitors, this transformation has an obvious merit of reducing the number of inductors.

The lumped elements in the transformed filter can be determined by the original filter and the variable t as follows:

$$L'=\frac{1}{tC} \tag{9}$$

$$C'=\frac{1}{tL} \tag{10}$$

An example of the CT filter in Fig. 2(a) and its transformed CT filter in Fig. 2(b) is shown in Table 1.

Fig. 3 plots the characteristics of the transmission zero and poles of the original filter and its transformed filter in Table 1. The transmission zeros originally in the lower stopband migrate to the upper stopband due to the cross-coupling. Similar change can be observed in the poles, which results in the filter passband to be controllable with t.

2.3. Enhanced resonator of type I

Adding poles or transmission zeros is a popular solution for filters with poor out-of-band rejection. The former implies usage of more resonators, whereas the latter means more cross-coupling or mix coupling, thereby resulting in usage of more inductors [25]. In this subsection, an approach of adding an extra transmission zero without additional usage of inductors is proposed.

Note that

$$|S_{11}|^2+|S_{12}|^2=1 \tag{11}$$

Based on (2) and (11), S_{11} and S_{12} can be expressed as

$$S_{11}=-\frac{\det(B_n)}{\det(C_n)} \tag{12}$$

$$|S_{12}|^2=1-\left|\frac{\det(B_n)}{\det(C_n)}\right|^2$$

Table 1
A transformed filter.

Original filter of Fig. 2(a)					
Element	C_1 (pF)	C_2 (pF)	C_3 (pF)	C_{12} (pF)	C_{13} (pF)
Value	36.8	75.8	65.7	41.95	12.65
	L_1 (nH)	L_2 (nH)	L_3 (nH)	L_{23} (nH)	
	0.0214	0.0172	0.0369	0.0309	
Transformed filter of Fig. 2(b) (herein, t is set to 1)					
Element	C_1 (pF)	C_2 (pF)	C_3 (pF)	C_{23} (nH)	L_1 (nH)
Value	46.73	58.14	27.1	32.36	0.0272
	L_2 (nH)	L_3 (nH)	L_{12} (nH)	L_{13} (nH)	
	0.0132	0.0152	0.024	0.08	

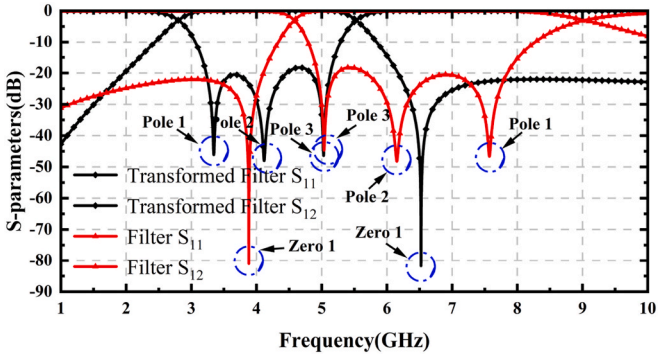

Fig. 3. S-parameters of the CT filter and the transformed CT filter.

$$= 1-\left|1+2jf_1\Big/\left[(m_{11}-j)f_1+\sum_{i=2}^{n}m_{1i}f_i\right]\right|^2 \tag{13}$$

with

$$B_n=\begin{bmatrix} m_{11}+j & m_{12} & \cdots & m_{1,n-1} & m_{1,n} \\ m_{12} & m_{22} & \cdots & m_{2,n-1} & m_{2,n} \\ \vdots & \vdots & \ddots & \vdots & \vdots \\ m_{1,n-1} & m_{2,n-1} & \cdots & m_{n-1,n-1} & m_{n-1,n} \\ m_{1,n} & m_{2,n} & \cdots & m_{n-1,n} & m_{n,n}-j \end{bmatrix} \tag{14}$$

$$C_n=\begin{bmatrix} m_{11}-j & m_{12} & \cdots & m_{1,n-1} & m_{1,n} \\ m_{12} & m_{22} & \cdots & m_{2,n-1} & m_{2,n} \\ \vdots & \vdots & \ddots & \vdots & \vdots \\ m_{1,n-1} & m_{2,n-1} & \cdots & m_{n-1,n-1} & m_{n-1,n} \\ m_{1,n} & m_{2,n} & \cdots & m_{n-1,n} & m_{n,n}-j \end{bmatrix} \tag{15}$$

where f_i is the cofactor of matrix B_n excluding the first row and ith column.

A simple mathematical relationship can be obtained from (12). When m_{11} tends to infinity, S_{12} tends to 0. According to the transformation of highpass filter to the bandstop filter given in Ref. [25], replacing the grounded inductor in the resonator with a grounded series inductor and capacitor allows the resonator to create an additional transmission zero. It should be noted that this replacement does not involve frequency transformation. Instead, its purpose is to generate transmission zeros.

The modified resonator, called the enhanced resonator of type I, is shown in Fig. 4(a). The transmission zero is generated at frequency $1/\sqrt{L_{1l}C_{1l}}$ by the enhanced resonator of type I. The self-coupling of the modified resonator can be expressed as

$$m_{11}=\omega C_1-\frac{\omega C_{1l}}{\omega^2 L_{1l}C_{1l}-1}+\sum_{j=2}^{n}C_{1j}-\sum_{j=2}^{n}\frac{1}{\omega L_{1j}} \tag{16}$$

where C_{ij} and L_{ij} are compensations for the negative component of the admittance inverter.

Taking the fourth-order circuit in Fig. 4(b) as an example, it can be regarded as a cascade of the enhanced resonator of type I and the circuit in Fig. 2(b), or a direct modification of the original fourth-order circuit in Fig. 4(c). Fig. 4(d) shows the additional transmission zero produced by the circuit in Fig. 4(b) by comparison to the circuit in Fig. 4(c). The values of the lumped elements for implementing the circuits in Fig. 4(b) and (c) are listed in Table 2.

2.4. Enhanced resonator of type II

Based on the circuit of Fig. 2(b), which is obtained after the frequency transformation, an enhanced resonator, called the enhanced resonator of type II, can be constructed as shown in Fig. 5(a).

According to the (12), S_{11} of the enhanced resonator can be

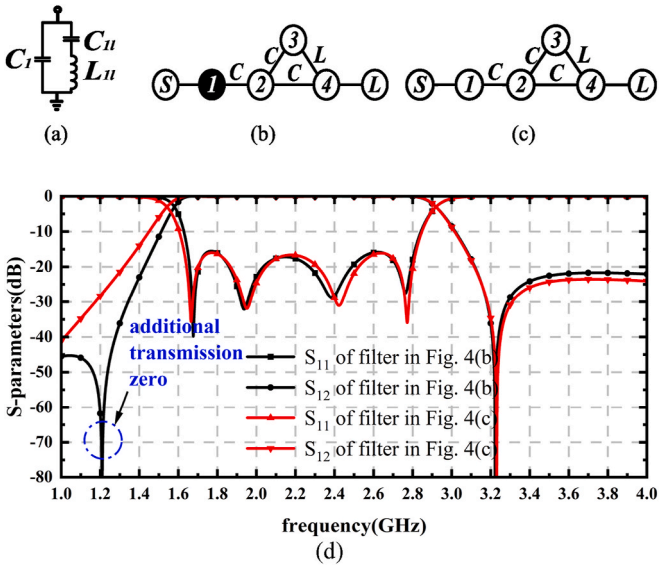

Fig. 4. (a) Enhanced resonator of type I. (b) Fourth-order filter with the enhanced resonator of type I. (c) Original fourth-order filter. (d) S-parameters of the filters in (b) and (c).

expressed as

$$S_{11}=\frac{\mathrm{Re}(B_3)+j\mathrm{Im}(B_3)}{\mathrm{Re}(C_3)+j\mathrm{Im}(C_3)} \tag{17}$$

where $Re(B_3)$, $Im(B_3)$, $Re(C_3)$, $Im(C_3)$ can be obtained from (14) and (15) as

$$\mathrm{Re}(B_3)=\begin{bmatrix} m_{11} & m_{12} & m_{13} \\ m_{12} & m_{22} & m_{23} \\ m_{13} & m_{23} & m_{33} \end{bmatrix}+m_{22}$$

$$\mathrm{Im}(B_3)=j\begin{vmatrix} m_{22} & m_{23} \\ m_{23} & m_{33} \end{vmatrix}-j\begin{vmatrix} m_{11} & m_{12} \\ m_{12} & m_{22} \end{vmatrix}$$

$$\mathrm{Re}(C_3)=\begin{bmatrix} m_{11} & m_{12} & m_{13} \\ m_{12} & m_{22} & m_{23} \\ m_{13} & m_{23} & m_{33} \end{bmatrix}-m_{22}$$

$$\mathrm{Im}(C_3)=-j\begin{vmatrix} m_{22} & m_{23} \\ m_{23} & m_{33} \end{vmatrix}-j\begin{vmatrix} m_{11} & m_{12} \\ m_{12} & m_{22} \end{vmatrix}$$

When both $Re(B_3)=0$ and $Im(B_3)=0$ are satisfied, the resonator can produce a pole. Taking into account the compensation of the negative component of the admittance inverter, as shown in Fig. 1(c), the coupling terms of this resonator can be expressed as (18).

$$m_{11}=\omega(C_{12}+C_{13})-\frac{1}{\omega L_1}$$

$$m_{22}=\omega(C_2+C_{12})-\frac{1}{\omega L_{23}}$$

$$m_{33}=\omega(C_3+C_{13})-\frac{1}{\omega L_{23}}$$

$$m_{12}=-\omega C_{12}, m_{13}=-\omega C_{13}, m_{23}=\frac{1}{\omega L_{23}} \tag{18}$$

According to 18, $Re(B_3)$ and $Im(B_3)$ can be characterized as (19). The poles of this resonator can be characterized as (20).

$$\begin{cases} \mathrm{Re}(B_3)=a_1x^2+b_1x+c_1 \\ \mathrm{Im}(B_3)=a_1x^2+b_1x-1 \end{cases} \tag{19}$$

$$\omega=\sqrt{\frac{a_2c_1+a_1}{a_1b_2-a_2b_1}} \tag{20}$$

Note that this resonator contains a cross-coupling, specifically represented as m_{13}, which can achieve a transmission zero. According to (2), S_{12} of this resonator can be expressed as (21).

$$S_{12}=-2j\frac{\begin{vmatrix} m_{12} & m_{13} \\ m_{22} & m_{23} \end{vmatrix}}{|A|} \tag{21}$$

According to the (21) and (18), the transmission zero of the enhanced resonator can be expressed as (26).

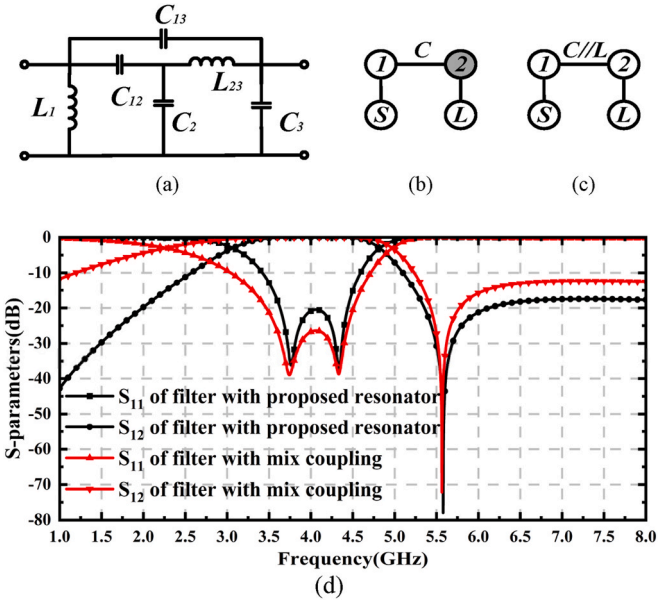

Fig. 5. (a) Enhanced resonator of type II. (b) Second-order filter with the enhanced resonator of type II. (c) Original second-order filter with mix coupling. (d) S-parameters of the circuits shown in (b) and (c).

Table 2
A filter with enhanced resonator of type I.

Filter of Fig. 4(b)							
Element	C_1 (pf)	C_2 (pf)	C_3 (pf)	C_4 (pf)	C_{11} (pf)	C_{12} (pf)	C_{23} (pf)
Value	35.9	168.25	142.1	112.25	205.8	103.95	82.6
	C_{24} (pf)	l_2 (nH)	l_3 (nH)	l_4 (nH)	l_{11} (nH)	l_{34} (nH)	
	36.8	0.0018	0.028	0.067	0.084	0.0576	
Filter of Fig. 4(c)							
Element	C_1 (pf)	C_2 (pf)	C_3 (pf)	C_4 (pf)	C_{12} (pf)	C_{23} (pf)	C_{24} (pf)
Value	92	150.25	109.25	112.5	101.25	75	112.5
	l_1 (nH)	l_2 (nH)	l_3 (nH)	l_4 (nH)	l_{34} (nH)		
	0.0035	0.0194	0.0374	0.0629	0.063		

$$\omega = \sqrt{\frac{C_{12}+C_{13}}{L_{23}(C_2+C_{12})C_{13}}} \tag{22}$$

By virtue of the enhanced resonator of type II and the circuit of Fig. 4 (c)–a novel second-order filter circuit, as shown in Fig. 5(b), can be formed by replacing resonators 2, 3, and 4 in Fig. 4(c) with the enhanced resonator of type II. The original second-order filter, which is formed by mix coupling of the resonators in Fig. 1(b)–is shown in Fig. 5(c). Note that both the filter circuits in Fig. 5(b) and (c) use the same number of inductors and have exactly two poles and one transmission zero. With the enhanced resonator type II, more capacitors can be implemented while maintaining the same number of used inductors. The designed filter based on this enhanced resonator of type II can achieve better out-of-band rejection.

Fig. 5(d) plots the S-parameters of the circuits in Fig. 5(b) and (c). The values of the lumped elements that realize Fig. 5(b) and (c) are listed in Table 3. From Fig. 5(d), one can observe that the novel filter with the enhanced resonator of type II exhibits superiority over the original one.

3. Validation and measurement

By cascading the enhanced resonators of type I and type II, a novel filter, as shown in Fig. 6(a), can be constructed. Type I resonators use only one inductor to produce one pole and one transmission zero which can reduce the usage of inductors. Type II resonators can achieve better out-of-band rejection with the same number of used inductors which can avoid using more inductors for high out-of-band rejection. In the IPD designs, inductors are one of the key components which occupy the largest physical area of the final design and result in high insertion loss. And by cascading these two resonators can effectively reduce the physical dimensions and insertion loss of the final filter designs.

This novel filter is designed and fabricated on a glass substrate with a relative permittivity of $\varepsilon = 4.4$ and a thickness of $h = 230$ μm. This novel filter is implemented using octagonal planar spiral inductors and MIM capacitors by virtue of the glass-based IPD technology. Fig. 6(b) shows the layout of this novel filter, which is designed using a full-wave electromagnetic solver, UltraEM [26].

Fig. 6(c) depicts the simulation and measure results of this novel filter. From Fig. 6(c), one can observe that this novel filter exhibits a bandwidth covering the range of $3.3-4.5$ GHz with an insertion loss less than 1.0 dB and a return loss less than -18 dB. Its out-of-band rejection is better than 25 dB at the low frequency band from 1.0 GHz to 2.5 GHz and better than 23 dB at the high frequency band from 6.0 GHz to 7.0 GHz.

From the measurement results, this novel filter has two poles in the passband and one transmission zero in the upper and lower stopbands. The measurement results are highly consistent with the simulation results. The physical size of this novel filter is $0.78 \times 1.08\ \text{mm}^2$ only, which is a half of the third-order cascade filter with two transmission zeros in Ref. [19]. The proposed design method can reduce the filter size and thus improve the chip integration. It enriches the freedoms during the filter design.

Table 4 summarizes the proposed filters and the reported high-performance filters. In comparison with [27,28,29], the designed filter based on the proposed method can achieve lower insertion loss. In comparison with [28,29], the designed filter can achieve a smaller physical size. In contrast to Refs. [28,30], the designed filter can utilize fewer inductors using the proposed method.

Table 3
A filter with enhanced resonator of type II.

Filter of Fig. 5(b)					
Element	C_1 (pF)	C_3 (pF)	C_4 (pF)	C_{12} (pF)	C_{23} (pF)
Value	12.06	56.5	62	26.5	52.65
	C_{24} (pF)	L_1 (nH)	L_2 (nH)	L_{34} (nH)	
	20.85	0.0604	0.0266	0.0263	
Filter of Fig. 5(c)					
Element	C_1 (pF)	C_2 (pF)	C_{12} (pF)	L_1 (nH)	L_2 (nH)
Value	49.65	58.3	62.45	0.0507	0.0393
	L_{13} (nH)				
	0.0131				

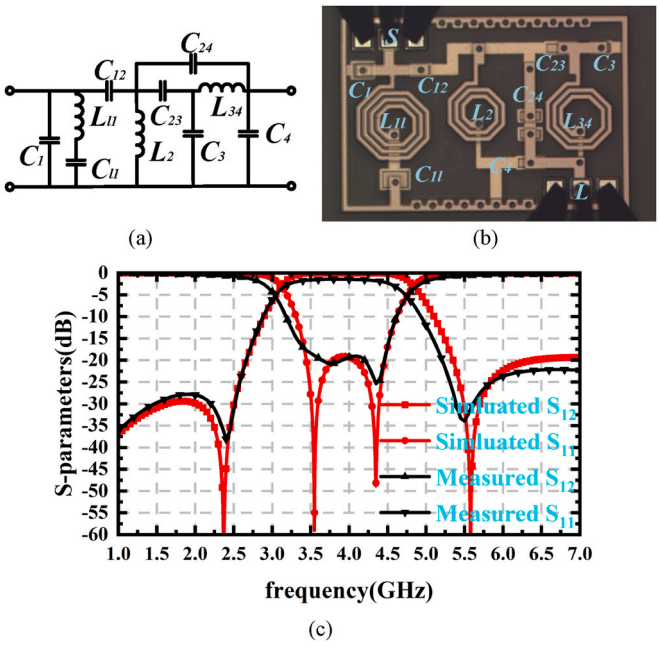

Fig. 6. (a) Novel filter with the enhanced resonators of type I and type II, where $C_1 = 0.5215pf$, $C_{l1} = 1.7066pf$, $C_3 = 1.2922pf$, $C_4 = 1.4173pf$, $C_{12} = 0.606pf$, $C_{23} = 1.204pf$, $C_{24} = 0.477pf$, $L_{l1} = 3.452nH$, $L_2 = 1.52nH$, $L_{34} = 1.502nH$. (b) Layout of the novel filter. (c) Simulation and measurement results.

4. Conclusion

Inductors that are widely used in wideband filter designs could result in large filter size and high insertion loss. Herein, a design method was proposed for wideband BPFs to reduce the use of inductors by analyzing the characteristics of coupling matrix based on the cascade filters. This design method, which is based on modified cascade filters implemented with direct lumped components, can achieve high performance of wideband BPFs with fewer inductors. In this design method, a frequency transformation and two enhanced resonators were proposed. To validate this design method, a novel filter was designed and fabricated using a glass-based IPD technology. It was shown that this design method can reduce the filter size and thus improve the chip integration, which provides a very promising approach for designing filter chips that have strict requirements on size and integration.

Author statement

Please find submitted the revised version of ID MEJ-D-24-00608, entitled “A Novel Design Method for Wideband Bandpass Filters with

Table 4
Comparison with reported filters.

Ref.	FBW	f_0(GHz)	IL(dB)	Size(mm^2)	Inductors
[27]	31 %	3.59	2	1.203 × 1.24	4
[28]A1	19.6 %	3.28	2.61	2.58 × 1.23	8
[30]	66 %	2.85	1.77	1.63 × 0.62	6
[29]	143 %	3	1.35	2.16 × 0.99	4
[22]	20 %	3	3.1	1.55 × 0.92	5
This work	31.2 %	3.85	1	1.08 × 0.78	3

Fewer Inductors", co-authored by J. Xing, H. Li, M. Xu, G. Wang, and me.

We have incorporated the reviewers' comments into the revised manuscript. We highly appreciate the valuable time and pertinent remarks and suggestions from you and the reviewers, which have surely made this manuscript better quality.

Finally, we would like to thank both you and the reviewers for spending time and efforts on this reviewing process.

Declaration of competing interest

The authors declare that they have no known competing financial interests or personal relationships that could have appeared to influence the work reported in this paper.

Data availability

No data was used for the research described in the article.

References

[1] Z. Zhu, J. Wang, A compact high-performance programmable-gain analog front end for HomePlug AV2 communication in 0.18- μm CMOS, IEEE Transactions on Circuits and Systems I: Regular Papers 64 (11) (Nov. 2017) 2858–2870.

[2] B. Liu, R. Zhou and Z. Zhu, "Reconfigurable 2.4/5.0-GHz dual-band CMOS power amplifier for WLAN 802.11ax," in IEEE Transactions on Circuits and Systems I: Regular Papers.

[3] H. Xu, et al., Large-range spurious mode elimination for wideband SAW filters on $LiNbO_3/SiO_2/Si$ platform by $LiNbO_3$ cut angle modulation, IEEE Trans. Ultrason. Ferroelectrics Freq. Control 69 (11) (Nov. 2022) 3117–3125.

[4] Ken-ya Hashimoto, X. Li, J. Bao, L. Qiu, T. Omori, Perturbation analysis of non linearity in radio-frequency bulk acoustic wave resonators using the mass-spring model, IEEE Trans. Ultrason. Ferroelectrics Freq. Control 67 (7) (July 2020) 1479–1484.

[5] Y.-C. Lin, T.-S. Horng, H.-H. Huang, Synthesizing a multiband LTCC bandpass filter with specified transmission- and reflection-zero frequencies, IEEE Trans. Microw. Theor. Tech. 62 (12) (Dec. 2014) 3351–3361.

[6] F.-J. Chen, X. Cheng, L. Zhang, Y.-L. Tian, Y. Tang, X.-J. Deng, Synthesis and design of lumped-element filters in GaAs technology based on frequency- dependent coupling matrices, IEEE Trans Microw. Theory. Techn. 67 (4) (April 2019) 1483–1495.

[7] X. Liu, Z. Zhu, Y. Liu, Q. Lu, X. Yin, Y. Yang, Compact bandpass filter and diplexer with wide-stopband suppression based on balanced substrate-integrated waveguide, IEEE Trans. Microw. Theor. Tech. 69 (1) (Jan. 2021) 54–64.

[8] X. Liu, Y. Liu, T. Zhang, Q. Lu, Z. Zhu, Substrate-integrated waveguide band-pass filter and diplexer with controllable transmission zeros and wide-stopband, IEEE Transactions on Circuits and Systems II: Express Briefs 70 (2) (Feb. 2023) 526–530.

[9] C. Fan, X. Liu, N. Liu and Z. Zhu, "Compact bandpass filters with low loss and TZs based on 1/n mode circle-SIW in through silicon vias (TSVs) technology," in IEEE Transactions on Microwave Theory and Techniques.

[10] R.J. Cameron, General coupling matrix synthesis methods for Chebyshev filtering functions, IEEE Trans. Microw. Theory. Techn. 47 (4) (April 1999) 433–442.

[11] Y.-T. Kuo, J.-C. Lu, C.-K. Liao, C.-Y. Chang, New multiband coupling matrix synthesis technique and its microstrip implementation, IEEE Trans. Microw. Theory. Techn. 58 (7) (July 2010) 1840–1850.

[12] X. Fan, S. Li, P.D. Laforge, Q.S. Cheng, A dualband coupling matrix method for designing quad-channel diplexer. 2019 IEEE MTT-S International Conference on Numerical Electromagnetic and Multiphysics Modeling and Optimization (NEMO), 2019, pp. 1–4. Boston, MA, USA.

[13] V. Miraftab, M. Yu, Generalized lossy microwave filter coupling matrix synthesis and design using mixed technologies, IEEE Trans. Microw. Theory. Techn. 56 (12) (Dec. 2008) 3016–3027.

[14] S. Pflüger, C. Waldschmidt, V. Ziegler, Coupling matrix extraction and reconfiguration using a generalized isospectral flow method, IEEE Trans. Microw. Theory. Techn. 64 (1) (Jan. 2016) 148–157.

[15] S. Amari, G. Macchiarella, Synthesis of inline filters with arbitrarily placed attenuation poles by using nonresonating nodes, IEEE Trans. Microw. Theory. Techn. 53 (10) (Oct. 2005) 3075–3081.

[16] P. Zhao, M. Rao, Design and tuning of extracted-pole filters with non-resonant nodes by circuit model extraction, IEEE Trans. Microw. Theory. Techn. 70 (4) (April 2022) 2174–2184.

[17] P. Dutta, G.A. Kumar, G. Ram, Numerical design of non-reciprocal bandpass filters with the aid of 3D coupling matrix for 5G bands, IEEE Transactions on Circuits and Systems II: Express Briefs 69 (7) (July 2022) 3334–3338.

[18] A. Alvarez-Melcon, X. Wu, J. Zang, X. Liu, J.S. Gomez-Diaz, Coupling matrix representation of nonreciprocal filters based on time-modulated resonators, IEEE Trans. Microw. Theory. Techn. 67 (12) (Dec. 2019) 4751–4763.

[19] Q. Zhang, C. Caloz, Synthesis of nonreciprocal lossless two-port networks using coupling matrix techniques. 2015 1st URSI Atlantic Radio Science Conference (URSI AT-RASC), Gran Canaria, Spain, 2015, 1-1.

[20] L. Szydlowski, N. Leszczynska, A. Lamecki, M. Mrozowski, A substrate integrated waveguide (SIW) bandpass filter in a box configuration with frequency-dependent coupling, IEEE Microw. Wireless Compon. Lett. 22 (11) (Nov. 2012) 556–558.

[21] L. Szydlowski, A. Lamecki, M. Mrozowski, Coupled-resonator waveguide filter in quadruplet topology with frequency-dependent coupling – a design based on coupling matrix, IEEE Microw. Wireless Compon. Lett. 22 (11) (Nov. 2012) 553–555.

[22] F.-J. Chen, X. Cheng, L. Zhang, Y.-L. Tian, Y. Tang, X.-J. Deng, Synthesis and design of lumped-element filters in GaAs technology based on frequency- dependent coupling matrices, IEEE Trans. Microw. Theory. Techn. 67 (4) (April 2019) 1483–1495.

[23] S. Amari, F. Seyfert, M. Bekheit, Theory of coupled resonator microwave bandpass filters of arbitrary bandwidth, IEEE Trans. Microw. Theory. Techn. 58 (8) (Aug. 2010) 2188–2203.

[24] B. Liu, K. Li, X. Chen, P.-L. Chi, T. Yang, Synthesis of wideband bandpass filter with cross-coupled or inline topology for direct circuit implementation using lumped elements, IEEE Trans. Microw. Theor. Tech. 72 (1) (Jan. 2024) 737–749.

[25] J.-S. Hong, M.J. Lancaster, Microstrip Filters for RF/Microwave Applications, Wiley, NY, USA, 2001. New Y ork.

[26] V.2023 UltraEM, Faraday Dynamics, Inc., Hangzhou, Zhejiang, China, 2023.

[27] W. Chen, Y. Wu, Y. Yang, W. Wang, IPD-based miniaturized wideband bandpass filter with frequency-dependent complex source and load, IEEE Trans. Plasma Sci. 49 (3) (March 2021) 1115–1120.

[28] Y. Xu, Y. Wu, H. Wu, Y. Yang, W. Wang, Wideband high selectivity filter chips with adjustable bandwidth based on IPD technology, IEEE Transactions on Circuits and Systems II: Express Briefs 69 (11) (Nov. 2022) 4273–4277.

[29] Y.-P. Lyu, Y.-J. Zhou, L. Zhu, C.-H. Cheng, Compact and high-order on-chip wideband bandpass filters on multimode resonator in integrated passive device technology, IEEE Electron. Device Lett. 43 (2) (Feb. 2022) 196–199.

[30] Y. Jiang, et al., Bandpass filter with ultra-wide upper stopband on GaAs IPD technology, IEEE Transactions on Circuits and Systems II: Express Briefs 69 (2) (Feb. 2022) 389–393.